Monolayer 2D semiconducting tellurides for high-mobility electronics

Huta R. Banjade, Jinbo Pan, and Qimin Yan*
Department of Physics, Temple University, Philadelphia, Pennsylvania 19122, USA

(Received 29 May 2020; revised 16 December 2020; accepted 23 December 2020; published 19 January 2021)

Discovery and design of two-dimensional (2D) materials with suitable band gaps and high carrier mobility are of vital importance for the photonics, optoelectronics, and high-speed electronics. In this work, based on first principles calculations using density functional theory with Perdew-Burke-Ernzerhof and Heyd-Scuseria-Ernzerhoffunctionals, we introduce a family of monolayer isostructural semiconducting tellurides $MNTe_4$, with $M = \{Ti, Zr, Hf\}$ and $N = \{Si, Ge\}$. These compounds have been identified to possess direct band gaps from 1.0 to 1.31 eV, which are well suited for photonics and optoelectronics applications. Additionally, anisotropic in-plane transport behavior is observed, and small electron and hole (0.11–0.15 m_e) effective masses are identified along the dominant transport direction. Ultrahigh carrier mobility is predicted for this family of 2D compounds, which host great promise for potential applications in high-speed electronic devices. Detailed analysis of electronic structures reveals the origins of the promising properties of this unique class of 2D telluride materials.

DOI: 10.1103/PhysRevMaterials.5.014005

I. INTRODUCTION

The successful fabrication of graphene [1,2], which is the first synthesized two-dimensional (2D) material, has initiated an exciting research field of 2D materials and functional devices. Great efforts have been focused on the discovery and synthesis of 2D materials, such as transition metal dichalcogenides (TMDCs) [3,4] and black phosphorus (BP) [5,6]. Successful fabrication of field-effect transistors, photodetectors, and light-emitting diodes using these 2D materials has demonstrated their potential for usage in electronics. These 2D materials possess remarkable properties that are absent in their bulk counterparts and have great application potential in optoelectronics, nanoelectronics, and ultrathin flexible devices [7]. Also, the presence of Dirac-cone structures and singularities in the electronic spectra of many predicted 2D materials make them promising for both fundamental research and potential electronic applications [8,9].

The field-effect transistor (FET) is the most successful device concept and a vital component of modern semiconductor electronics. Carrier mobility of the channel material and its band gap play an essential role in the performance of FETs [10], such as on-off ratio and operation speed, and the identification of novel channel materials in FET technology is a significant task in semiconductor electronics. At room temperature, graphene exhibits extremely high carrier mobility (10 000–15 000 $cm^2\ V^{-1}\ s^{-1}$) [11], which has ignited great excitement in the device community as a possible channel material in FETs. However, the gapless electronic structure and related low on/off ratio of graphene transistors hinder their application for logic operation [12]. Tremendous efforts have been applied to open a sizable band gap in graphene. Unfortunately, the creation of a band gap has always been accompanied by a dramatic decrease in mobility [11].

With the successful fabrication of high-performance MoS_2 FETs [13], the search for novel 2D materials for electronics gained more momentum. FETs made from few layer TMDC's such as MoS_2 and WSe_2 exhibit high on/off current ratios and excellent current saturation characteristics, but the carrier mobility ($<200\ cm^2\ V^{-1}\ s^{-1}$ at room temperature) [14–16] is much smaller than that of graphene. Recent studies show that another 2D semiconductor, single layer black phosphorus (phosphorene), exhibits high carrier mobility ($\sim 1000\ cm^2\ V^{-1}$ s [1] at room temperature) [6,17], but is still orders of magnitude less in comparison to graphene. Hence, the search for stable and semiconducting 2D materials as graphene alternatives that can outperform the silicon-based devices is worthwhile and will be an excellent boon for the electronic device community.

In this work, we propose a family of MNX_4 type 2D monolayer semiconductors with a suitable band gap, low carrier effective mass, and potentially high carrier mobility along the dominant propagation direction. We perform the first principles calculations on a family of 2D ternary group-IV chalcogenides consisting of 36 MNX_4 compounds, with M as (Ti, Zr, Hf) from group IV, N as (Si, Ge) from group XIV, and X as (S, Se, or Te) from group XVI of the periodic table. Among those 36 compounds, we found that six telluride compounds with the chemical formula $MNTe_4$ are very promising due to their direct band gaps, strong in-plane anisotropy, and low carrier effective masses along the major transport direction.

Compounds with similar structure and composition, including $ZrGeTe_4$, $HfGeTe_4$, and $TiGeTe_6$, have already been synthesized in their bulk form [18], and the measurement of their structural information and other intrinsic properties such as electrical conductivity and magnetic susceptibility has been

*qiminyan@temple.edu

 ©2021 American Physical Society

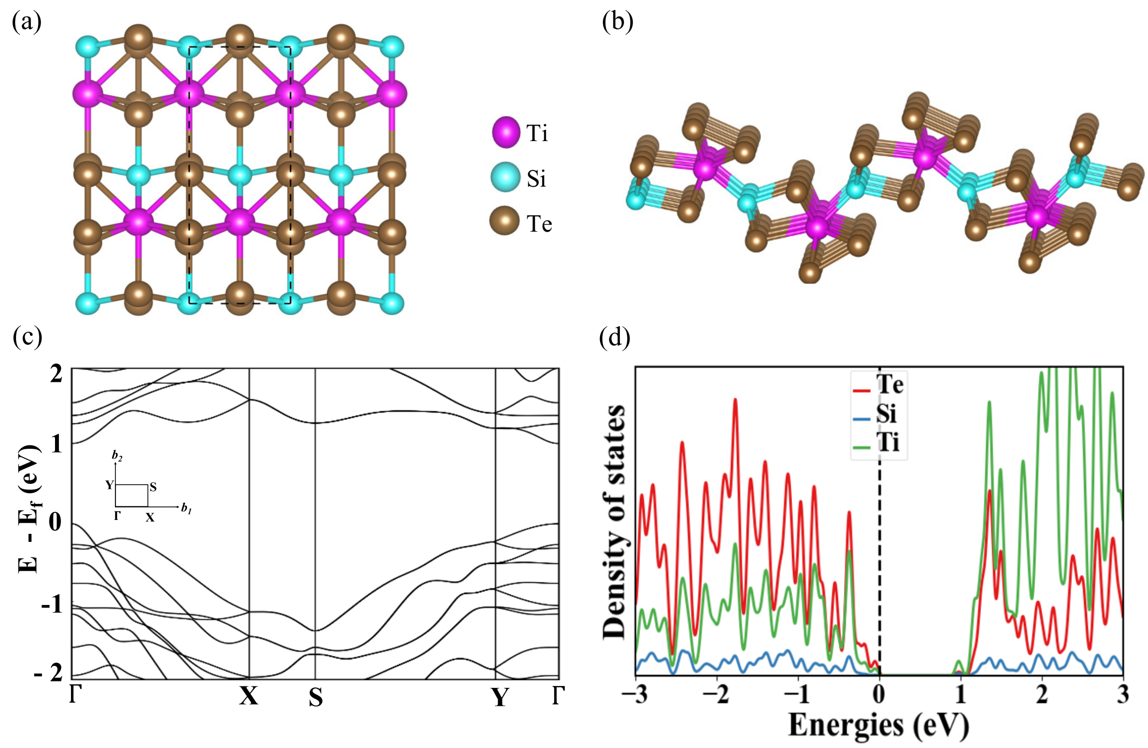

FIG. 1. (a) Top and (b) side view of the relaxed structure of TiSiTe4. The magenta, cyan, and brown balls represent Ti, Si, and Te atoms, respectively. (c) Band structure of TiSiTe4 calculated on the level of HSE06 hybrid functional. High-symmetry *k* points in the reciprocal space are presented in the figure. (d) Projected density of states of $TiSiTe_4$, showing that the dominant states at the CBM and VBM are contributed by Ti *d* states and Te *p* states, respectively.

performed [18]. According to the Materials Project database [19], the bulk phase of $ZrGeTe_4$ is thermodynamically stable in the Zr-Ge-Te phase diagram, which provides a strong motivation for experimental synthesis efforts. The atomic structure of these semiconducting tellurides (MNX_4) is characterized by the presence of metal-centered bicapped trigonal prisms as a fundamental structural unit, a ubiquitous feature in ternary group-V chalcogenides, coordinated by a "metal-metal" bond between atom *M* (transition metal) and *N* (group XIV), as shown by the relaxed structure of $TiSiTe_4$ in Fig. 1. Owing to this unique bonding structure, these 2D semiconducting tellurides exhibit many promising electronic properties, which are of vital importance in applications such as optoelectronics [20], nanoelectronics [7], and ultrathin flexible devices [20,21].

II. COMPUTATIONAL DETAILS

The geometry optimization and electronic structure calculations are performed by using density functional theory (DFT) as implemented in the Vienna *ab initio* simulation package (VASP) [22]. The projected-augmented-wave (PAW) pseudopotentials [23,24] are used to describe the valence electron and core interactions. Generalized gradient approximation (GGA) [25,26] and the Perdew-Burke-Ernzerhof (PBE) [27] exchange-correlation functional are used to describe the electron exchange-correlation. DFT calculations are performed at the PBE level to identify the trends in band structures and extract effective masses, through which we identify six telluride compounds with high carrier mobilities based on their band structures and effective masses. It is well known that the local/semilocal functional based DFT method severely underestimates the band gaps of semiconducting or insulating solids [28]. To partially address the band gap problem, all the electronic structure calculations on the six telluride compounds are performed by using the Heyd-Scuseria-Ernzerhof hybrid functional (HSE) [29,30]. A $9 \times 3 \times 1\Gamma$-centered *k*-point mesh and a plane-wave energy cutoff of 400 eV are used, which provide well-converged results. All atoms are relaxed until the final force exerted on each atom is less than 0.01 eV/Å and the change in total energy between the two steps is less than 10^{-4} eV.

Figures 1(b) and 1(c) illustrate the typical electronic band structure and atomic projected density of states (PDOS) of $TiSiTe_4$ as an outstanding example of the ternary 2D telluride family (see band structures and projected density of states for all other compounds in Figs. S1 and S2 in the Supplemental Material [31]). A detailed study of band structure shows that conduction band minima (CBM) and valence band maxima (VBM) lie at the center of the Brillouin zone, i.e., the Γ point, indicating that a direct transition between CBM and VBM is plausible. Our hybrid functional calculations show that there are sizable direct band gaps in these 2D compounds, ranging from 1.00 eV in $TiGeTe_4$ to 1.31 eV in $HfSiTe_4$. Predicted values of band gaps, along with relaxed lattice constants, are presented in Table I. To test the effect of spin-orbit coupling (SOC) in the electronic structures of the compounds, we perform the PBE+SOC band structure calculations for those compounds with relatively heavy atoms (Hf and Zr). Figure S3 shows the electronic band structure of the

TABLE I. Relaxed lattice constants (a and b) and the computed band gaps estimated by using the HSE06 functional.

	Lattice constant (Å)		
Compounds	a	B	Band gap (eV)
$HfGeTe_4$	3.99	10.99	1.29
$HfSiTe_4$	3.96	10.85	1.31
$TiGeTe_4$	3.90	10.76	0.99
TiSiTe4	3.87	10.61	1.03
ZrGeTe4	4.01	11.04	1.23
ZrSiTe4	3.97	10.90	1.24

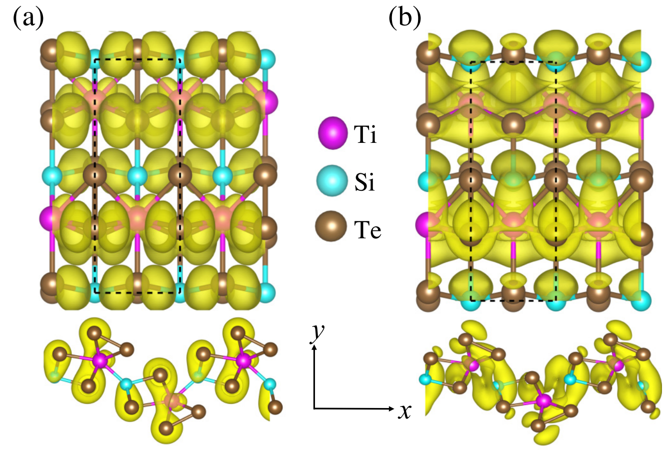

FIG. 2. Top and side view of band decomposed partial charge density of $TiSiTe_4$ at (a) the VBM and (b) the CBM at Γ point in the x-y plane at the $0.0064e$ Å^{-3} isosurface level. The magenta, cyan, and brown balls represent Ti, Si, and Te atoms, respectively.

compounds $HfSiTe_4$ and $ZrSiTe_4$. The inclusion of SOC has no appreciable effect on the primary features such as the band dispersion at both CBM and VBM. Large dispersion in both conduction and valence bands close to Γ indicates the lower carrier effective mass along the dominant transport direction. Because of the variation in dispersion in the band along the dominant transport direction, the anisotropic effect can be observed in the band structure, and hence the anisotropic transport behavior of charge carriers is expected.

Electron and hole effective masses for these 2D telluride compounds are estimated by using the parabolic fitting of the energy bands around CBM and VBM near the Γ point in k space. Effective masses of electrons and holes span a wide range from $0.11\,m_0$ to $1.26\,m_0$ along the dominant transport direction, where m_0 is the electron rest mass. Predicted values of effective masses for electrons and holes along the Γ-X and Γ-Y directions are presented in Table II. Variation in the calculated effective masses along the two in-plane directions indicate the strong anisotropic electric transport in these materials. This anisotropic transport behavior is similar to that of black phosphorene [6]. The PDOS in these compounds shows that the valence band maxima are mostly dominated by Te p states, while the conduction band minima are mainly constructed by transition metal (i.e., M) d states, with the presence of strong hybridization between atoms M and N in some compounds. For instance, Fig. 1(c) shows the PDOS for $TiSiTe_4$, in which the valence band maxima are dominated by Te p states while the conduction band minima are dominated by Ti d states. Consistent with this observation, the band decomposed partial charge density (Fig. 2) for the electronic state at the VBM and CBM in $TiSiTe_4$ is localized at Te and Ti atoms respectively. Detailed analysis of band decomposed partial charge densities for all other compounds are presented in the Supplemental Material (Fig. S4).

Electronic properties of mono to several layer 2D semiconductors are mainly governed by carrier mobilities. We estimate the carrier mobilities theoretically for the family of 2D tellurides along with the two in-plane transport directions (Γ-X and Γ-Y) based on the theoretical approach proposed by Bardeen *et al.* with an acoustic-phonon-limited scattering model [32]. Note that the optical phonon contribution is not included in this model, and hence the theoretically predicted mobilities estimated by this model can be considered as an upper limit for the experimentally achievable mobility. Due to the inverse relationship between mobility and effective mass, a small effective mass is obviously one of the preliminary requirements for high carrier mobility. In addition to carrier effective mass, other important factors affecting the mobilities include the deformation potentials and the elastic

TABLE II. Effective mass m_x^* (m_y^*), deformation potential E_{1x}(E_{1y}), 2D Elastic modulus c_{x2D}(c_{y2D}), and the carrier mobility $\boldsymbol{\mu}_x$ ($\boldsymbol{\mu}_y$) along the dominant transport direction Γ-X and Γ-Y for the electron (e) and hole (h) carriers.

Compound		m_x^* (m_0)	m_y^* (m_0)	E_{1x} (eV)	E_{1y} (eV)	c_{x2D} (Jm^{-2})	c_{y2D} (Jm^{-2})	μ_0(10^3 cm^2 V^{-1} s^{-1})	μy(10^3 cm^2 V^{-1} s^{-1})
$HfGeTe_4$	e	0.28	0.35	3.55	3.58	87.25	45.75	1.70	0.70
	h	0.11	1.13	9.00	2.27	87.25	45.75	0.60	0.47
$HfSiTe_4$	e	0.25	0.43	2.58	2.29	77.21	53.41	3.10	1.54
	h	0.12	1.01	9.85	1.99	77.21	53.41	0.40	0.82
$ZrGeTe_4$	e	0.30	0.32	3.62	3.03	77.49	39.17	1.36	0.92
	h	0.12	1.21	9.37	2.02	77.49	39.17	0.41	0.45
$ZrSiTe_4$	e	0.29	0.44	1.68	2.01	77.47	50.46	5.58	1.68
	h	0.15	1.12	9.52	1.90	77.47	50.46	0.30	0.65
$TiSiTe_4$	e	0.33	0.29	1.28	3.46	77.40	62.50	9.92	1.24
	h	0.14	1.07	9.79	2.55	77.40	62.50	0.32	0.49
$TiGeTe_4$	e	0.38	0.22	2.10	4.30	67.83	51.69	2.98	0.94
	h	0.13	1.26	9.848	2.47	67.83	51.69	0.29	0.35

modulus along the propagation direction of longitudinal acoustic waves [6].

In this work, the carrier mobility of 2D materials is estimated by a simplified relation [6]: $\mu_{x(y)} = \frac{e\hbar^3 C_{x(y)2D}}{k_B T m_e^* m_d (E_1^i)^2}$, where $m_d = \sqrt{(m_x^{i*} m_y^{i*})}$ is the average effective mass, i represents the electron for the conduction band or hole for the valence band (subscripts x and y indicate the Γ-X and Γ-Y transport directions), $m_e{}^*$ is the carrier effective mass, T is the temperature (room temperature $T = 300$ K is used), $E_1{}^i$ stands for the deformation potential along the transport direction, and $C_{x(y)2D}$ is the 2D elastic modulus along the transport direction. The deformation potential for both electrons and holes along the x and y directions is obtained by the linear fitting of band energy at the CBM and VBM with respect to strains along Γ-X and Γ-Y. The 2D elastic modulus is calculated using the relation $(E - E_0)/S_0 = C_{x(y)2D}(\Delta l/l_0)^2/2$, where E_0 is the total energy and S_0 is the lattice area at equilibrium for the 2D system, l_0 is the equilibrium lattice constant along the transport direction, and Δl is its change due to strain. The calculation details of deformation potential, 2D elastic modulus, and fitted curves for change in band edge and total energy for all compounds are presented in the Supplemental Material (Fig. S5). Note that no imaginary frequency is observed in the phonon spectra [33] (see Fig. S6 in the Supplemental Material), which indicates the thermal stability of monolayer MNX_4 compounds.

Computed values of effective masses, deformation potentials, 2D elastic modulus, and carrier mobilities for all the 2D telluride compounds are presented in Table II. Carrier mobilities in these compounds range from hundreds to almost tens of thousands of $\mathrm{cm^2\,V^{-1}\,s^{-1}}$, which endows this family of 2D compounds with a great potential for electronic and optoelectronic applications. These carrier mobilities exhibit high in-plane directional anisotropy, with electrons being more mobile in general. Even though the electron effective mass ($0.33m_0$ in $TiSiTe_4$ and $0.19m_0$ in $ZrSiTe_4$) along the Γ-X direction is slightly larger compared with other known 2D compounds for electronic applications, the computed electron mobility along the x direction is extremely large in $TiSiTe_4$ and $ZrSiTe_4$ due to the rather small absolute deformation potentials for the conduction band along the x direction. The calculated results show that holes are more mobile along Γ-Y (except in $HfGeTe_4$).

As carrier mobilities are highly correlated with the deformation potentials, the understanding of the anisotropy in deformation potentials is essential. Since the computed electron mobility in these compounds is higher along the Γ-X direction, here we focused ourselves in understanding the difference in deformation potential related to the strain along the x direction via the VBM and CBM wave functions and bonding analysis between neighboring atoms utilizing the projected crystal orbital Hamiltonian population (pCOHP) as incorporated in the LOBSTER package [34]. pCOHP is a powerful physical quantity to understand the details of bonding, nonbonding, and antibonding interactions between pair of atoms and their atomic orbitals in a compound [35]. Here we present the −pCOHP in which a positive value corresponds to the bonding state and a negative value corresponds to the antibonding state.

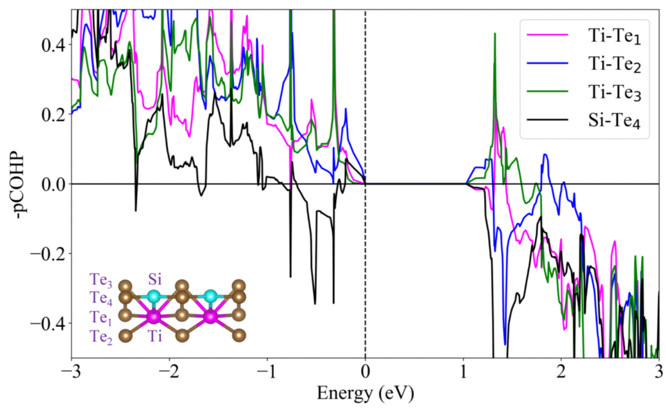

FIG. 3. Projected crystal orbital Hamiltonian population (−pCOHP) between neighboring atoms of $TiSiTe_4$, with the corresponding structure showing the adjacent atoms of which pCOHP is obtained from.

As shown in Fig. 3, taking $TiSiTe_4$ as an example, there exists a strong bonding interaction between Ti/Si atoms and neighboring Te atoms along the x direction at the VBM. In contrast, a mixture of bonding and antibonding interaction is observed at the CBM. The VBM wave function in Fig. 2(a) shows a substantial overlap along the x direction, indicating that a small structural deformation along the x direction may have a remarkable effect on this electronic state and hence cause a significant change in its energy, resulting in a considerable deformation potential. The situation is somewhat different for the CBM wave function along the x direction, which exhibits much weaker orbital overlap [Fig. 2(b)]. As observed in Fig. 3(b), the mixture of bonding and antibonding interaction between neighboring atoms along the x direction results in a dramatic decrease in the overall strength of the orbital interaction. Due to this effect, structural deformation has much less impact on the CBM wave function along the x direction, which results in the smaller values of deformation potential. Along the y direction, the VBM wave functions [as shown in Fig. 2(a)] are more localized than the CBM wave functions [Fig. 2(b)], resulting in smaller values of deformation potential at the VBM than those at the CBM along the y direction. Similar bonding and antibonding interactions are observed for other compounds in the family. For instance, a similar pCOHP for $ZrSiTe_4$ is shown in Fig. S7 in the Supplemental Material. As the nature of anisotropy in the observed deformation potentials is similar in these compounds, we conclude that this anisotropic transport behavior is dominated by the bonding and antibonding interaction between the neighboring atomic orbitals and their different response under strain. Mobility along a transport direction is inversely proportional to the square of the deformation potential along that direction. Therefore, the mobility along a transport direction is actively controlled (but not fully determined) by the deformation potential in that direction. The observed higher electron mobilities along the x direction in these telluride compounds are mostly due to the lower values of deformation potential at the CBM along the x direction. Besides, these predicted mobilities can be viewed as an upper limit for the experimentally achievable mobility.

In summary, we predict a family of 2D ternary semiconducting tellurides with the chemical composition $MNTe_4$ by using first principles computations based on density functional theory. Computed band gaps and carrier mobilities of this compound set exhibit great potentials for electronic and optoelectronic applications. All these compounds possess direct band gaps at the center of Brillouin zone (i.e., Γ point) with extremely high electron mobilities higher than that of single layer BP, MoS_2, and other 2D MX_2 semiconductors. Out of these six compounds, we present two benchmark systems: $TiSiTe_4$ with a band gap at 1.03 eV and electron mobility at $9.92 \times 10^3\ cm^2\ V^{-1}\ s^{-1}$ and $ZrSiTe_4$ with a band gap at 1.24 eV and electron mobility at $5.58 \times 10^3\ cm^2\ V^{-1}\ s^{-1}$, which are promising for logical devices that require high mobility and optimal band gap. Like single layer BP, the observed anisotropy in mobility in these compounds is mainly due to the anisotropy in deformation potential, which is correlated with the bonding-antibonding interactions between neighboring atomic orbitals and a subsequently different response of the CBM and VBM under strain. The computational identification of these 2D telluride compounds provides a material platform for experiments in the search for functional materials that enable future 2D electronic devices.

ACKNOWLEDGMENTS

This work was supported by the U.S. Department of Energy, Office of Science, under Award No. DE-SC0020310. It benefitted from the supercomputing resources of the National Energy Research Scientific Computing Center (NERSC), a U.S. Department of Energy Office of Science User Facility operated under Contract No. DE-AC02-05CH11231, and by the U.S. Army Research Laboratory under Contract No. W911NF-16-2-0189.

[1] K. S. Novoselov, A. K. Geim, S. V. Morozov, D. Jiang, Y. Zhang, S. V. Dubonos, I. V. Grigorieva, and A. A. Firsov, Electric field effect in atomically thin carbon films, Science **306**, 666 (2004).

[2] K. S. Novoselov, D. Jiang, F. Schedin, T. J. Booth, V. V. Khotkevich, S. V. Morozov, and A. K. Geim, Two-dimensional atomic crystals, Proc. Natl. Acad. Sci. USA **102**, 10451 (2005).

[3] D. Jariwala, V. K. Sangwan, L. J. Lauhon, T. J. Marks, and M. C. Hersam, Emerging device applications for semiconducting two-dimensional transition metal dichalcogenides, ACS Nano **8**, 1102 (2014).

[4] Q. H. Wang, K. Kalantar-Zadeh, A. Kis, J. N. Coleman, and M. S. Strano, Electronics and optoelectronics of two-dimensional transition metal dichalcogenides, Nat. Nanotechnol. **7**, 699 (2012).

[5] A. Yuichi, E. Shoichi, and N. Shin-ichiro, Electrical properties of black phosphorus single crystals, J. Phys. Soc. Jpn. **52**, 2148 (1983).

[6] J. Qiao, X. Kong, Z.-X. Hu, F. Yang, and W. Ji, High-mobility transport anisotropy and linear dichroism in few-layer black phosphorus, Nat. Commun. **5**, 4475 (2014).

[7] P. Miró, M. Audiffred, and T. Heine, An atlas of two-dimensional materials, Chem. Soc. Rev. **43**, 6537 (2014).

[8] J. Wang, S. Deng, Z. Liu, and Z. Liu, The rare two-dimensional materials with Dirac cones, Natl. Sci. Rev. **2**, 22 (2015).

[9] Y.-F. Zhang, J. Pan, H. Banjade, J. Yu, T.-R. Chang, H. Lin, A. Bansil, S. Du, and Q. Yan, Two-dimensional MX family of Dirac materials with tunable electronic and topological properties, arXiv:2005.07365.

[10] F. Schwierz, J. Pezoldt, and R. Granzner, Two-dimensional materials and their prospects in transistor electronics, Nanoscale **7**, 8261 (2015).

[11] F. Schwierz, Graphene transistors, Nat. Nanotechnol. **5**, 487 (2010).

[12] K. Kim, J.-Y. Choi, T. Kim, S.-H. Cho, and H.-J. Chung, A role for graphene in silicon-based semiconductor devices, Nature (London) **479**, 338 (2011).

[13] B. Radisavljevic, A. Radenovic, J. Brivio, V. Giacometti, and A. Kis, Single-layer MoS_2 transistors, Nat. Nanotechnol. **6**, 147 (2011).

[14] H. Fang, S. Chuang, T. C. Chang, K. Takei, T. Takahashi, and A. Javey, High-performance single layered WSe_2 p-FETs with chemically doped contacts, Nano Lett. **12**, 3788 (2012).

[15] H. Wang, L. Yu, Y. H. Lee, Y. Shi, A. Hsu, M. L. Chin, L. J. Li, M. Dubey, J. Kong, and T. Palacios, Integrated circuits based on bilayer MoS_2 transistors, Nano Lett. **12**, 4674 (2012).

[16] B. Radisavljevic and A. Kis, Reply to 'Measurement of mobility in dual-gated MoS_2 transistors', Nat. Nanotechnol. **8**, 147 (2013).

[17] L. Li, Y. Yu, G. J. Ye, Q. Ge, X. Ou, H. Wu, D. Feng, X. H. Chen, and Y. Zhang, Black phosphorus field-effect transistors, Nat. Nanotechnol. **9**, 372 (2014).

[18] A. Mar and J. A. Ibers, The layered ternary germanium tellurides $ZrGeTe_4$, $HfGeTe_4$, and $TiGeTe_6$: Structure, Bonding, and Physical Properties, J. Am. Chem. Soc. **115**, 3227 (1993).

[19] A. Jain, G. Hautier, S. P. Ong, C. J. Moore, C. C. Fischer, K. A. Persson, and G. Ceder, Formation enthalpies by mixing GGA and GGA + U calculations, Phys. Rev. B **84**, 045115 (2011).

[20] C. Ataca, H. Şahin, E. Aktürk, and S. Ciraci, Mechanical and electronic properties of MoS_2 nanoribbons and their defects, J. Phys. Chem. C **115**, 3934 (2011).

[21] N. K. Nepal, L. Yu, Q. Yan, and A. Ruzsinszky, First-principles study of mechanical and electronic properties of bent monolayer transition metal dichalcogenides, Phys. Rev. Mater. **3**, 73601 (2019).

[22] G. Kresse and J. Furthmüller, Efficiency of ab-initio total energy calculations for metals and semiconductors using a plane-wave basis set, Comput. Mater. Sci. **6**, 15 (1996).

[23] P. E. Blöchl, Projector augmented-wave method, Phys. Rev. B **50**, 17953 (1994).

[24] G. Kresse and D. Joubert, From ultrasoft pseudopotentials to the projector augmented-wave method, Phys. Rev. B **59**, 1758 (1999).

[25] D. C. Langreth and M. J. Mehl, Beyond the local-density approximation in calculations of ground-state electronic properties, Phys. Rev. B **28**, 1809 (1983).
[26] J. P. Perdew, J. A. Chevary, S. H. Vosko, K. A. Jackson, M. R. Pederson, D. J. Singh, and C. Fiolhais, Atoms, molecules, solids, and surfaces: Applications of the generalized gradient approximation for exchange and correlation, Phys. Rev. B **46**, 6671 (1992).
[27] J. P. Perdew, K. Burke, and M. Ernzerhof, Generalized Gradient Approximation Made Simple, Phys. Rev. Lett. **77**, 3865 (1996).
[28] J. P. Perdew, Density functional theory and the band gap problem, Int. J. Quantum Chem. **28**, 497 (2009).
[29] J. Heyd, G. E. Scuseria, and M. Ernzerhof, Erratum: Hybrid functionals based on a screened Coulomb potential (Journal of Chemical Physics (2003) 118 (8207)), J. Chem. Phys. **124**, 219906 (2006).
[30] J. Heyd, G. E. Scuseria, and M. Ernzerhof, Hybrid functionals based on a screened Coulomb potential, J. Chem. Phys. **118**, 8207 (2003).
[31] See Supplemental Material at http://link.aps.org/supplemental/10.1103/PhysRevMaterials.5.014005 for analysis of the stability of the compounds, methods to compute the deformation potential, elastic modulus, and the effective masses. Band structures, the projected density of states, and the partial charge densities for all the compounds we studied.
[32] J. Bardeen and W. Shockley, Deformation potentials and mobilities in non-polar crystals, Phys. Rev. **80**, 72 (1950).
[33] A. Togo and I. Tanaka, First principles phonon calculations in materials science, Scr. Mater. **108**, 1 (2015).
[34] S. Maintz, V. L. Deringer, A. L. Tchougr, and R. Dronskowski, LOBSTER : A tool to extract chemical bonding from plane-wave based DFT, J. Comput. Chem. **37**, 1030 (2016).
[35] M. Esser, A. A. Esser, D. M. Proserpio, and R. Dronskowski, Bonding analyses of unconventional carbon allotropes, Carbon N. Y. **121**, 154 (2017).